Iridium nanostructured metal oxide, its inclusion in silica matrix and their activity toward photodegradation of methylene blue

C. Diaz*[a], M. L. Valenzuela[b], O. Cifuentes-Vaca[c], M. Segovia[a] and M. A. Laguna-Bercero *[d].

[a]*Departamento de Química, Facultad de Química, Universidad de Chile. La Palmeras 3425, Nuñoa, casilla 653, Santiago de Chile, Chile*

[b]*Universidad Autónoma de Chile, Instituto de Ciencias Químicas Aplicadas, Inorganic Chemistry and Molecular Material Center, Facultad de Ingeniería. Av. El Llano Subercaseaux 2801. San Miguel. Santiago de Chile.*

[c]*Facultad de Ciencias Exactas, Universidad Andrés Bello, Sede Concepción, Autopista Concepción-Talcahuano 7100, Talcahuano, Chile.*

[d]*Instituto de Ciencia de Materiales de Aragón (ICMA), CSIC- Universidad de Zaragoza C/ Pedro Cerbuna 12, E-50009, Zaragoza, Spain.*

ABSTRACT

Precious metal oxides of IrO_2 were prepared by thermal treatment of the macromolecular Chitosan●$(IrCl_3)_X$ and PSP-4-PVP●$(IrCl_3)_X$ precursors. Using this procedure, pure IrO_2, phases were formed. The nature of the polymeric precursor is acting as a solid state template and influences the size of the iridium dioxide but not significantly the morphology, and the obtained IrO_2 nanoparticles are about 15 nm. For the first time, the photocatalytic degradation of methylene blue using IrO_2 was measured founding a moderated activity. The inclusion of IrO_2 into SiO_2 was performed using a combined solution of the Chitosan and PVP precursors by the sol-gel method. Subsequent pyrolysis of the isolated solid-state Chitosan●$(IrCl_3)_x(SiO_2)_y$ and PSP-4-PVP●$(IrCl_3)x(SiO_2)_y$ give rise to the IrO_2//SiO_2 nanocomposites. The IrO_2 particles are distributed uniformly inside the matrix of SiO_2 leading to stable semi porous materials appropriate for high temperature catalytic applications. The IrO_2 nanoparticles formed from the PVP precursor are mainly nanobars of 10 nm width, while that for the chitosan precursor are around 25 nm. The IrO_2/SiO_2 composites exhibit a moderate photocatalytic activity toward the degradation of methylene blue and similar to that of IrO_2.

1. Introduction

Among the metals of the periodic table, the so called precious as among other, Ir, is one of the most catalytically active [1]. Their activity is hugely enhanced at the nano-level [2,3]. This metal, as well as their metal oxides, exhibits a high catalytic activity [1,3]. IrO_2 is a promising conducting oxide used for example as an electrode material in ferroelectric capacitors for nonvolatile memories applications [4]. Although isolated solution preparation methods for nanostructured Ir oxides are well documented [4-11], no solid-state general methods to prepare IrO_2 nanostructured have been reported. IrO_2 is generally prepared from an Ir salt. The relative fraction of IrO_2/Ir depends on the temperature, producing Ir_2O_3 at temperatures between 250 to 400 $^{\circ}$C, and then obtaining pure IrO_2 at temperatures above 600 $^{\circ}$C [4-11]. Here we report a general and suitable method for the preparation of nanostructured IrO_2 [12-14]. Regarding to the possible application of this Ir oxide, the first step is usually their incorporation in solid matrices. Additionally, when the application of these nanostructured metal oxides involves high temperatures, the metal oxide inside the matrix must be stable [15,16]. The incorporation of metal-oxide nanoparticles into solid devices is not straightforward [15,16] when produced via a solution phase method, as the solid-state isolation of the nanoparticles usually causes nanoparticle agglomeration [17-20]. Thus, the incorporation of metal-oxide nanoparticles generated directly from a solid-state approach appears to be the most reliable method.

A schematic representation of the macromolecular precursors is shown in scheme 1.

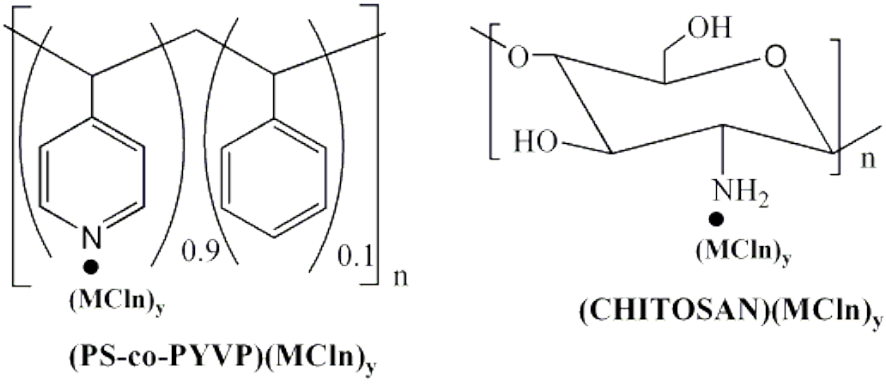

Scheme 1: General representation of complexes of polymer-metal structure.

The use of the photo-catalysts for environmental remediation is attracting much interest in recent years, as air and water pollution are possibly the major environmental risks to human health. In this sense, a wide number of novel approaches are being under continuous development, including for example polymeric graphitic carbon nitride (g-C_3N_4)-based semiconducting nanostructured materials [21], Cu2S@TiO2 core-shell nanostructures [22], Co-doped ZrO2 nanoparticles [23] or graphite–TiO_2 nanoparticle composites [24]. On the other hand, supported precious metal or metal oxides catalysts are widely used in industrial catalytic processes due to their superior catalytic performance [25,26]. Thermal deterioration including metal sintering is a primary cause for catalyst deactivation, especially under severe oxidizing atmosphere. A widely used support matrix for precious metal or metal oxides catalysts is silica [27]. In this work, we propose a reliable method to prepare nanoparticles of IrO_2 included in SiO_2. The addition of SiO_2 matrix was chosen not only for improving photocatalysis, but also for facilitating their synthesis. In any case, it was previously reported that the combination of SiO_2 with other photocatalysers such as TiO_2 can improve photocatalytic activity in the long term, and especially hydrophilicity [28,29]. An additional advantage is that the addition of SiO_2 also restricts the grain growth of metal oxide particles [30]. Stable nanocomposites (IrO_2)//SiO_2 are obtained by a high temperature thermal treatment of the solid precursors Chitosan●$(IrCl_3)_n$//SiO_2 and PS-co-4-PVP●$(IrCl_3)_n$//SiO_2, as seen in scheme 2.

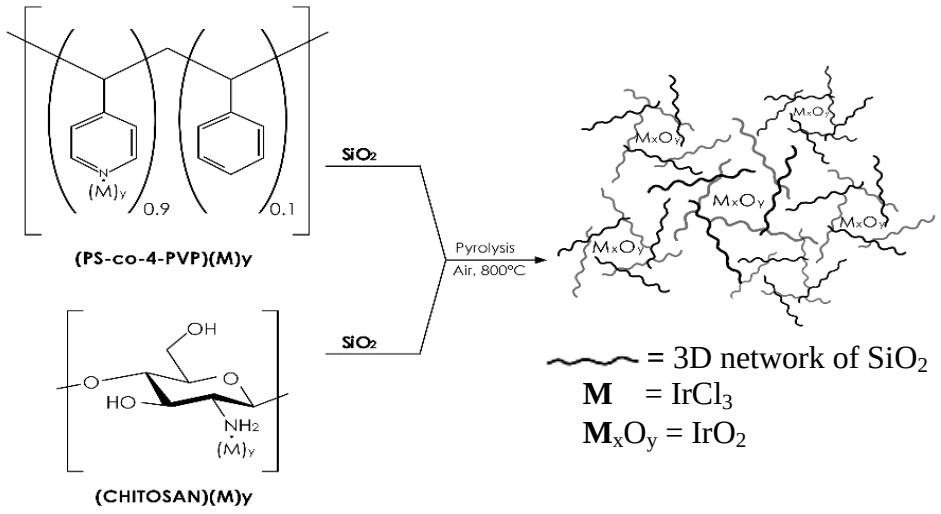

Scheme 2: General representation of the inclusion of the Ir, nanostructured metal oxide into SiO_2.

2. Experimental

Chemicals: Chitosan (low molecular weigt) IrCl3, PSP-4-PVP (with 10 % of pyridine groups), TEOS (98 %) were purchased from Sigma-Aldrich (St. Louis, US) and used as received. Dichloromethane (for analysis) and acetic acid (analytical grade. 99%) purchased from Merck (Darmstadt, Germany) were used as received. H_2O nanopure was obtained from distillated water, which was purified using a SG Labostar 4DI apparatus.

Preparation of complexes of polymer-metal: In 20 ml dichloromethane, a stoichiometric amount of the polymer (1:1 polymer:complex) and 0,40 g of metal complexes were added. The heterogeneous mixture was stirred at room temperature for 8 days. The as obtained solid was washed with dichloromethane and dried under vacuum during 3 hours. Additional details are given in Table 1 of the Supplementary Material.

Pyrolysis: The polymer-metal complexes were placed into a box furnace (lab tech) using a temperature program of pyrolysis at 800 ºC.

Preparation of complexes of polymer-metal//Silica: In 20 ml dichloromethane, a stoichiometric amount of the polymer (1:1 polymer: complex) and 0,40 g of metal complexes were added. The heterogeneous mixture was stirred a room temperature for 8 days and then silica sols were added. This was prepared by mixing TEOS (Tetraethyl orthosilicate), acetic acid and H_2O mili-Q (1:4:4 TEOS: Acetic Acid: H_2O) at room temperature under stirring for 5 hours. The resulting gel was dried in a vacuum-oven at 80 °C and then calcined at 800 ^{o}C. Additional details are given in Table 1 of the Supplementary Material. The composition of the as obtained nanostructured materials are shown in Table 1

Table 1
Yields, color and composition of the pyrolytic products from the respective precursors.

Precursor Polymer	Formula	Yield (%)	Color	Composition
(1)	PS-co-4-PVP●$(IrCl_3)_n$	53	black	IrO_2
(2)	Chitosan●$(IrCl_3)_n$	low	black	IrO_2
(3)	PS-co-4-PVP●$(IrCl_3)_n$//SiO_2	67	grey	IrO_2 /SiO_2
(4)	Chitosan●$(IrCl_3)_n$//SiO_2	68	grey	IrO_2 /SiO_2

Characterization: TG/DTA analyses were performed on a TGA 4000 Perking Elmer analyser. Scanning electron microscopy (SEM) was performed on a JEOL 5410 scanning electron microscope. Elemental microanalysis was performed by energy dispersive X-ray analysis using a NORAN Instrument micro-probe attached to the SEM. High-Resolution Transmission Electron Microscopy (HR-TEM) was performed using a JEOL 2000FX TEM microscope at 200 kV to characterize the average particle size, distribution and elemental and crystal composition. The images were analysed using the Digital Micrograph software. Methylene Blue (MB) was used as a model compound to test the photocatalytic properties at 655 nm under UV-Vis illumination using a xenon lamp (150W) positioned 20 cm away from the photoreactor in a range 330-680 nm at room temperature, to avoid the self-degradation and thermal catalytic effects of cationic MB dye.

3. Results and Discussion

The presence and the degree coordination of the $IrCl_3$ to the polymer backbone were performed by TG analysis under air. The pyrolytic residue corresponds to IrO_2. By mass difference and comparing with the macromolecular complex with a 100 % coordination, the estimated coordination degree values are 82% in **1** and 92% for **2**. TG analysis confirmed the presence of both Chitosan and PS-co-4-PVP slightly modified by coordination of the $IrCl_3$, see S2 in Supplementary Material. Additional characterization including UV-visible diffuse reflectance and Band gap analysis can be found in supplementary information S7.

XRD patterns of the as prepared IrO_2 from both precursors are shown in figure 1. For both polymer templates, it can be observed from the XRD patterns that only pure IrO_2 single phase was obtained, in concordance with other different preparation methods [5,6]. In addittion, it was found that when the pyrolysis was made in a a poor oxygen atmosphere, a mixture IrO_2/Ir was obtained.

SEM analysis for the pyrolytic product from PSP-4-PVP●$(IrCl_3)_X$ is shown in figure 2 (a) and (b), indicating a porous morphology. Interestingly, this porous structure has not been previously reported [4-10]. When chitosan is used as precursor, similar morphology, although slightly denser was observed, as seen in figure 2 c,d.

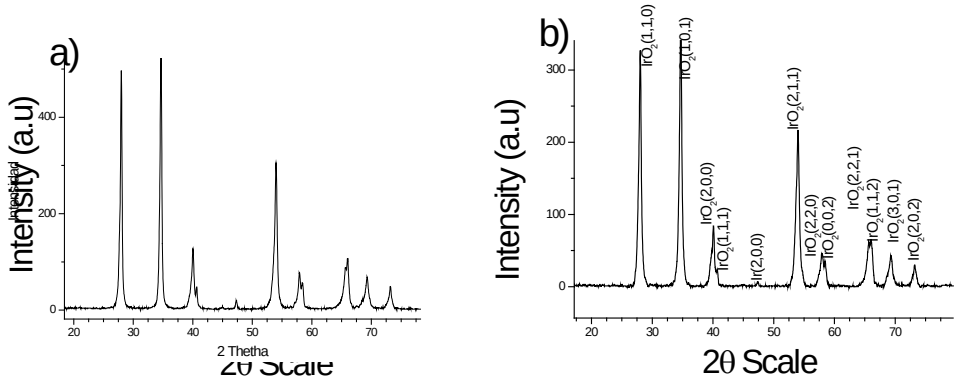

Fig. 1 XRD patterns of IrO_2 obtained from precursors: a) Chitosan●$(IrCl_3)_X$, b) PSP-4-PVP●$(IrCl_3)_X$.

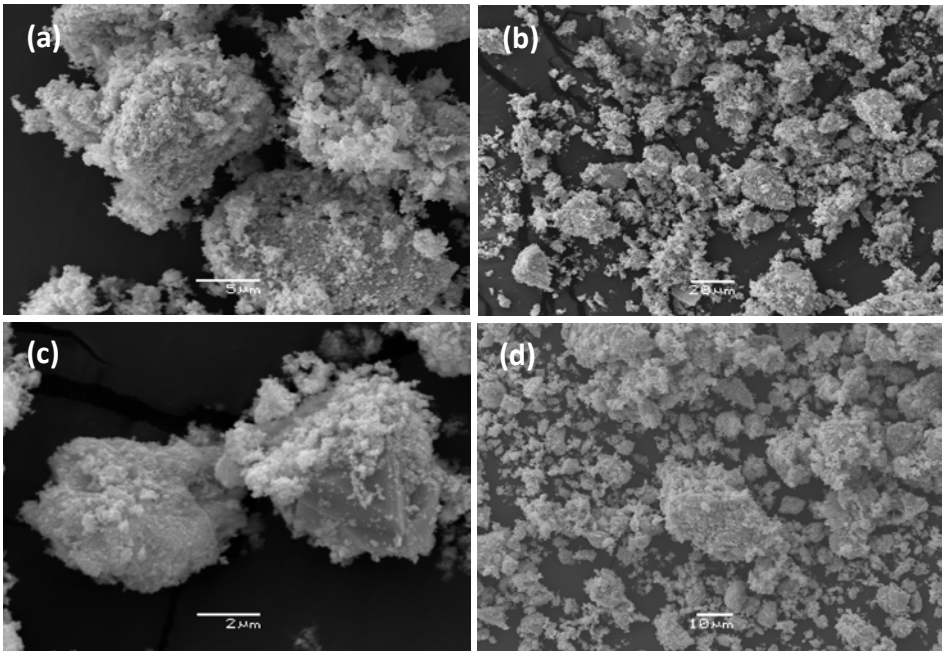

Fig. 2 SEM image for the IrO_2-PVP sample, a) and b); IrO_2-Chitosan sample c) and d)

A linear EDS scanning (figure 3) was performed to corroborate the presence of Ir (blue) and oxygen (green), which id consistent with IrO_2. This experiment also confirms the homogeneity of the sample. In addition, the presence of carbon (red in figure 3d and 3h) is associated to carbon traces from an incomplete carbonization of the respective template polymer.

HR-TEM analysis of the as obtained IrO_2 material from both chitosan and PVP precursors corroborate their crystalline structure, as shown in figure 4. Typical particle sizes are about 10-30 nm and 20-50 nm, for the chitosan and the PVP precursor, respectively. For example, interplanar distance of the 110 and 101 planes can be observed in figure 4a and 4b, respectively.

Similar results were obtained for the IrO_2 material obtained from the PVP precursor, where interplanar distance of the 110 plane can be observed in figure 4c. In addtion, an inset with the FFT is shown in figure 4 d, which corresponds to the [111] direction. Those resutls are

very relevant, as HR-TEM images were not previously reported for IrO_2 prepared from different solution methods [4-8].

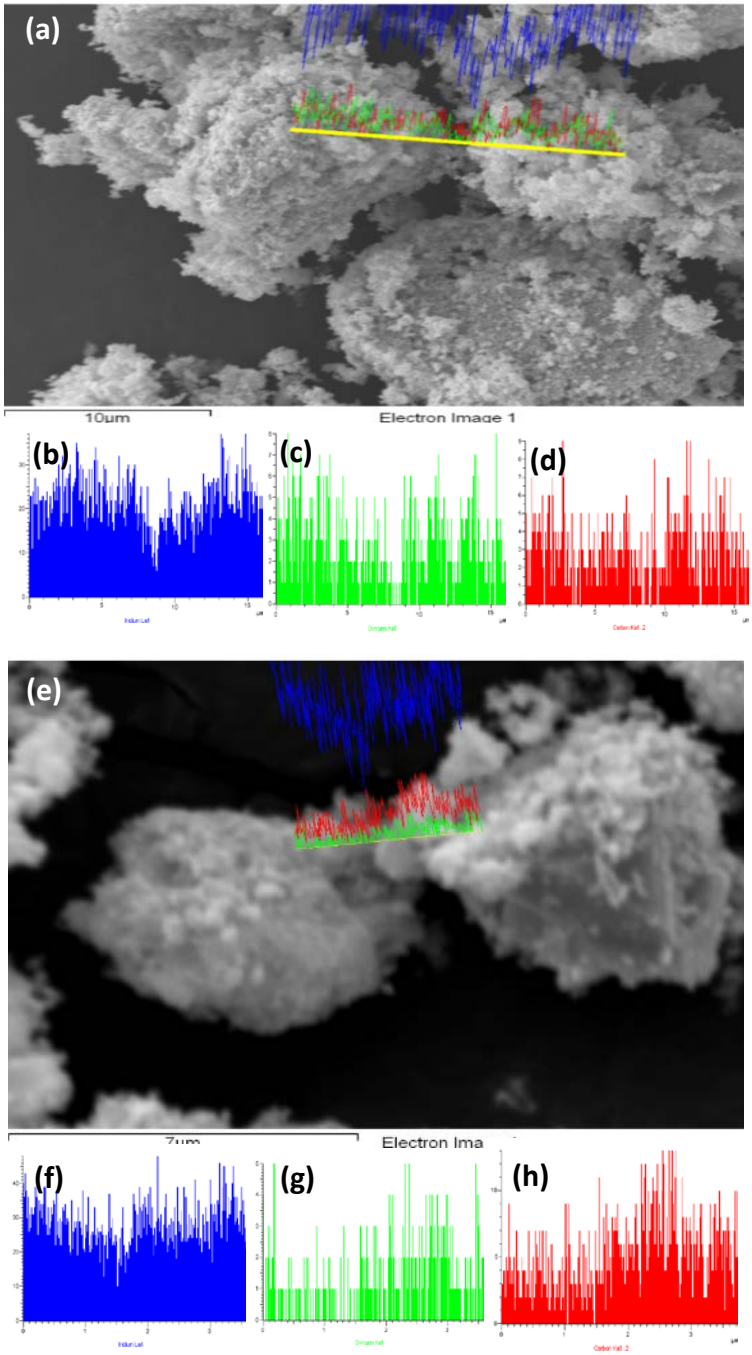

Fig. 3 Linear EDS scanning of iridium: (b) and (f); oxygen: (c) and (g); and carbon d) and h) for the pyrolytic product from PSP-4-PVP●$(IrCl_3)_X$ (a)-(d) and Chitosan●$(IrCl_3)_X$ (e)-(h), respectively.

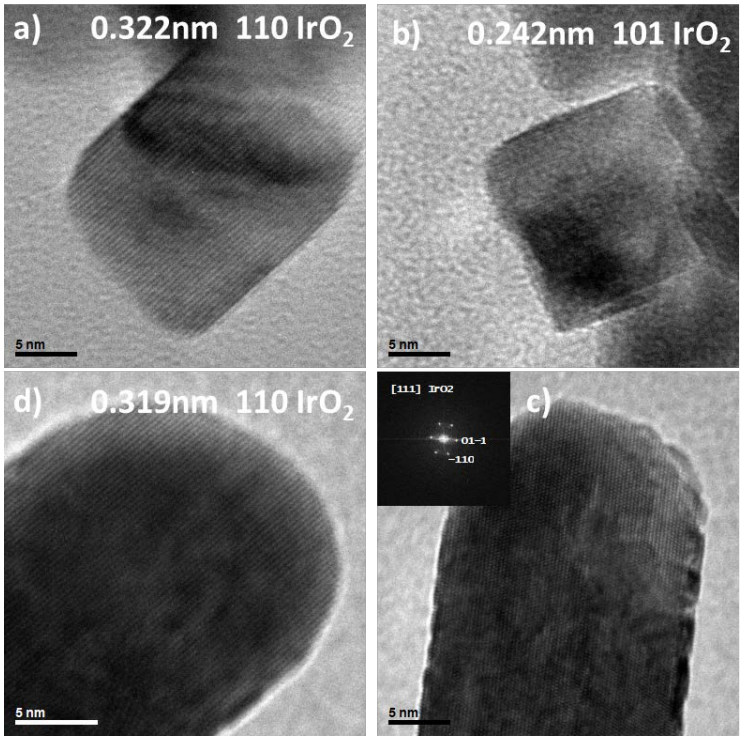

Fig. 4 HR-TEM of IrO2 particles from both Chitosan (a) and (b) and PVP (c) and (d) precursors.

In addition to the limitation about the preparation methods, all in solution, for IrO_2 [11], more limited are those for composites with SiO_2. In this work, we propose the incorporation of IrO_2 into SiO_2 gels by using the macromolecular Chitosan●$(IrCl_3)x$ and PSP-4-PVP●$(IrCl_3)_X$ precursors. The phase purity of the IrO_2//SiO_2 products was characterized by X-ray diffraction. For IrO_2//SiO_2 produced from the chitosan precursor, the XRD pattern observed in figure 5 presents a broad main peak of amorphous silica around $\theta = 21°$ [32-34] and the typical diffraction peaks of IrO_2 [5,6]. Similar XRD pattern diffraction was observed for the PVP precursor.

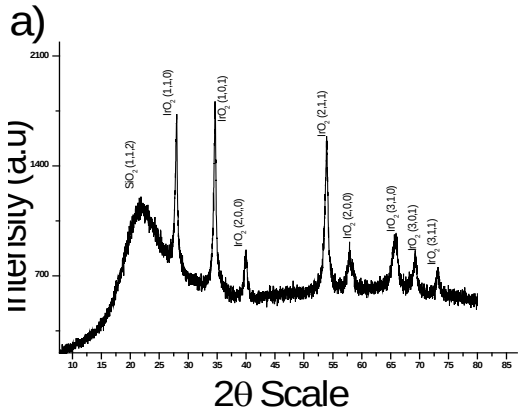

Fig. 5 XRD pattern of $IrO_2//SiO_2$ from Chitosan●$(IrCl_3)_X$ //SiO_2

TEM images for the $IrO_2//SiO_2$ sample obtained from the chitosan precursor are shown in figure 6 (a and b), where typical bar nanoparticles joined to the SiO_2 matrix can be observed. A similar morphology, although more randomly distributed can be observed for the $IrO_2//SiO_2$ nanocomposite obtained from the PVP precursor (see figures 6 c and d). Selected area diffraction pattern (SAED) analysis confirmed that the bar nanoparticles correspond to IrO_2. In addition, EDS analysis was also performed in these particles showing the presence of IrO_2 and in some cases the SiO_2 matrix, as shown in figures 6 f and h.

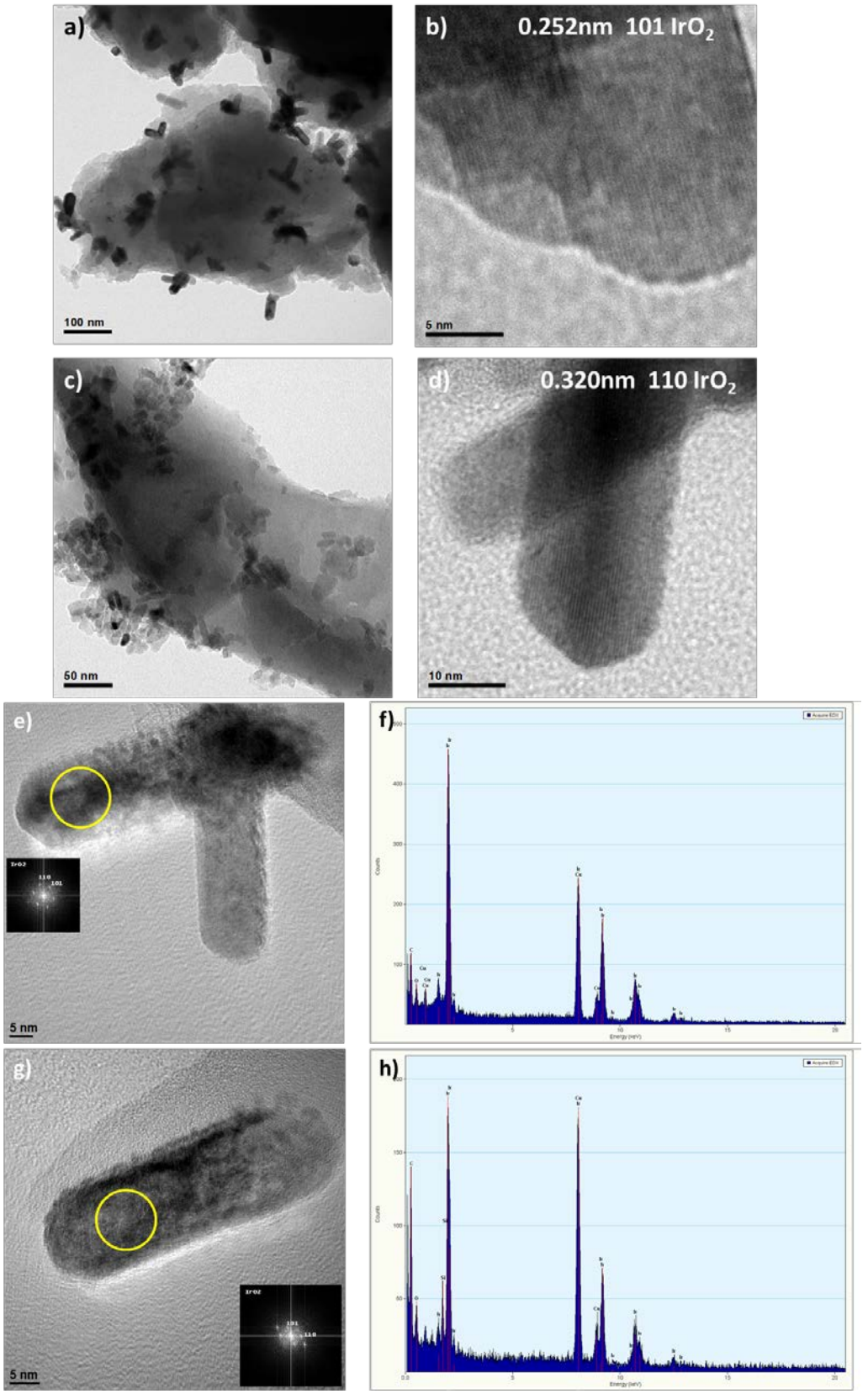
a)
100 nm
b)
0.252nm 101 IrO2
5 nm
c)
50 nm
d)
0.320nm 110 IrO2
10 nm
e)
5 nm
f)
g)
5 nm
h)

Fig. 6. HR-TEM analysis of IrO_2//SiO_2 obtained from the Chitosan (a)-(b)-(e) and PVP precursors (c)-(d)-(g). SAED patterns (e)-(g) and EDS analysis is also shown, which corresponds to the marked areas in figures (e) and (g).

Additional information about the uniform distribution of the IrO_2 nanoparticles inside silica was obtained by EDX mapping from SEM images, as shown in figure 7 for IrO_2//SiO_2.

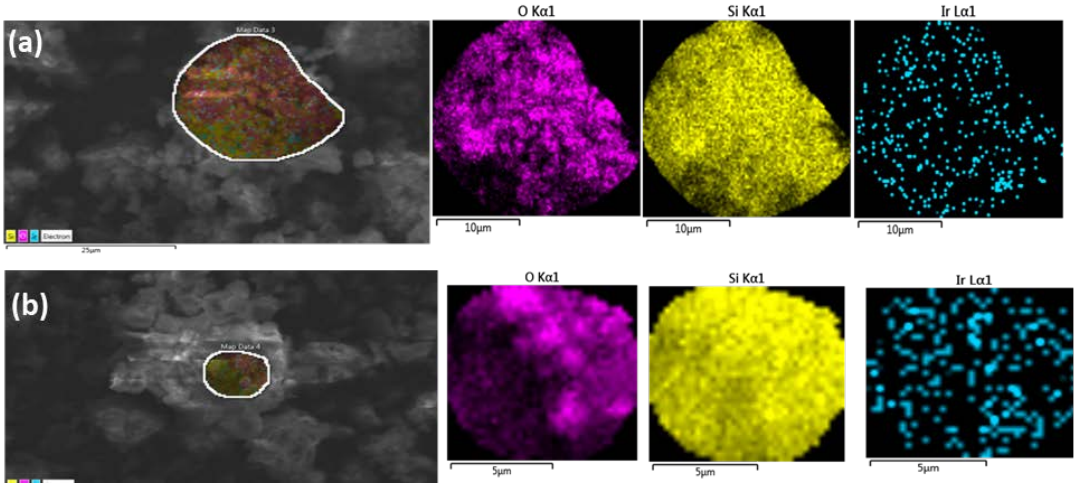

Fig. 7 EDX-elemental mapping of IrO_2 nanoparticles inside silica from precursor Chitosan●$(IrCl_3)_X$ //SiO_2 (a) and PSP-4-PVP●$(IrCl_3)_X$ //SiO_2 (b) precursors.

Photocatalytic behavior of IrO_2

Methylene blue (MB) is one of the extensively used organic dyes in coloring paper, temporary hair colorant, dyeing cotton and coating for paper stock [36, 37], and the state of the art photocatalyst material is based on TiO2 [38]. In this work, we have used this dye as a model dye to assay the photocatalytic properties of IrO_2. The removal of this hazardous dye is considered as one of the growing needs in recent years. The photocatalytic experiments were carried on the IrO_2 catalyst with defined concentrations under dark conditions and with UV irradiations in attempts to prove their efficiency. The absorption spectra vs time of the Ir oxides are shown in supporting information S3. Additional

information about the amount of adsorbed methylene blue before the photocatlytic process, and the effect of pH and cycle tests can be found in supporting information S8.

IrO_2 is a well-known electrically conductive material [4] and then it could have photodegradation properties in the UV range, as well as in the visible range. However, to the best of our knowledge, there is no report on their photocatalytic activity. The only related studies are those about the catalytic reduction of 4-Nitrophenol [9] and the electrochemical catalytic activity toward oxygen evolution [7]. The typical MB degradation rate for the IrO_2 obtained from both chitosan and PVP precursors are shown in figure 8 (a). IrO_2-PVP sample exhibits a better photocatalytic activity (57 % photodegradation in 300 minutes) than the IrO_2-Chitosan (38 % photodegradation in 300 minutes). This effect was associated to the more porous morphology of IrO_2-PVP sample, as previously discussed by SEM/TEM. In addition, the photocatalytic reaction of the IrO_2-Chitosan sample followed a first zero order kinetic as shown in figure 8 (b). A similar behavior was observed for the IrO_2-PVP sample (Supporting Information, see figure S4).

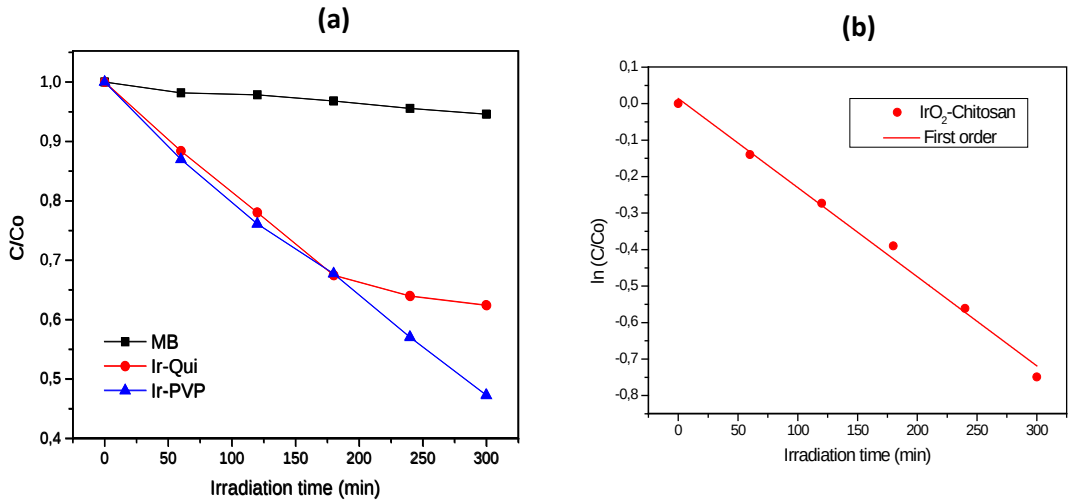

Fig. 8 (a) Normalized concentration changing of MB without catalyst, in presence of IrO_2 from the PSP-4-PVP●$(IrCl_3)_X$ and in presence of Chitosan●$(IrCl_3)_X$. (b) Normalized concentration changing of MB (C/C_0) vs. the irradiation time.

Photocatalytic behavior of **IrO_2/SiO_2 composites**

In order to compare the photocatalytic activity of IrO_2 with and without SiO_2, we have measured the degradation of methylene blue with IrO_2/SiO_2. Figure 9 shows the degradation plots of C/c_0 vs time for both composites observing a 53 % and 54 % MB degradation for PVP and chitosan, respectively. This activity is very similar to the one previously reported without inclusion of IrO_2 inside silica. These finding indicates that the SiO_2 matrix do not significantly changes the morphology of the IrO_2 nanoparticles. In addition, S5 shows the absorption spectra vs time of the IrO_2/SiO_2 composites, and the kinetic and absorbance of methylene blue vs of time is also given in the supplementary material (S6).

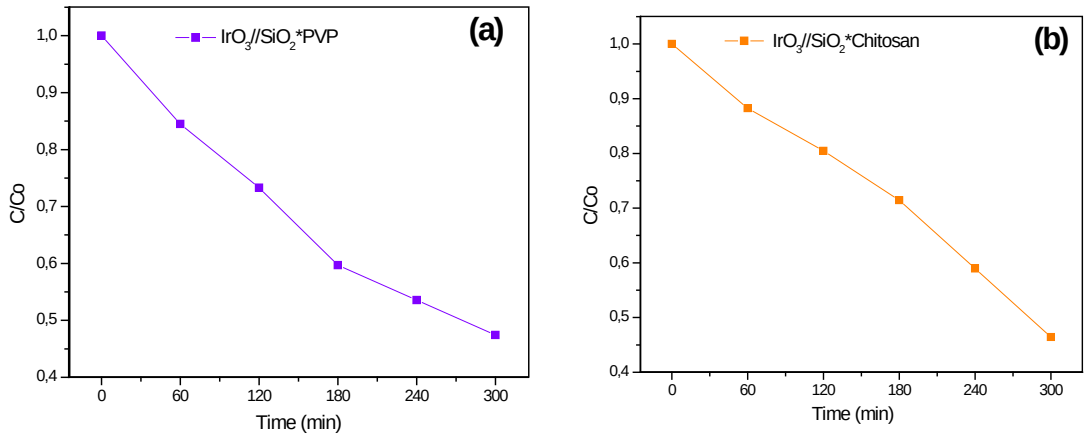

Fig. 9 Normalized concentration change of MB without catalyst, in presence of IrO_2/SiO_2-PVP (a) and in presence of IrO_2/SiO_2-Chitosan (b).

Table 2 summarizes the kinetic data for the degradation of MB with IrO_2-PS-4-PVP, IrO_2-Chitosan, and IrO_2/SiO_2--PS-4-PVP, IrO_2/SiO_2-Chitosan. As there are no previous literature reports for photodegradation of MB with IrO_2 and IrO_2/SiO_2 materials, a direct comparison is not possible. As reference, about 54% of MB was degraded after 120 min using identical conditions for commercial TiO_2 (Degussa P25) [38].

In addition, as observed from figure 9, it is observed that the IrO2/SiO2-chitosan compound presents higher percentages of degradation. However, its photodegradation rate constant is not proportional to this value. This observation could explain that the first order observed behavior indicates that the speed of the process is determined by the dynamic adsorption

equilibrium on the photogenerated active sites in the catalyst, which at low concentrations of the adsorbate (dye) depends only on the concentration in the solution. This is a constant of apparent speed since the process is intrinsically second order, involving both the concentration of dye and the active sites in the catalyst. Under the conditions in these experiments, the concentration of active sites is a constant (independent of what happens in solution), which is included in the observed rate constant.

Table 2: Kinetic data for the photodegradation process of MB with IrO_2, and IrO_2/SiO_2.

Photocatalyst	Photodegradation rate constant k ($10^{-3}M \cdot min^{-1}$)	Discoloration rate (%)	R^2 Linear fit (%)
IrO_2-PS-4-PVP	1,7	53%	0,995
IrO_2-Chitosan	2,4	38%	0,991
IrO_2/SiO_2-PS-4-PVP	2,5	53%	0,990
IrO_2/SiO_2-Chitosan	1,7	54%	0,991

Formation mechanism

In order to give some insight about the formation mechanism of the nanostructured IrO_2, we believe that materials from both precursors can be proposed using the mechanism of formation of nanostructured metallic materials from the oligomer precursor $\{NP(OC_8H_{12})_2(OC_6H_4PPh_2\text{-}Mn(CO)_2(\eta^5\text{-}C_5H_4Me)_2\}_n$ [39]. A schematic representation of this process is provided in figure 10. Briefly, the first step on heating involves the formation of a 3D network to produce a thermally stable matrix. This step is crucial because it offsets the sublimation. The first heating step could involve a cross linking of the chitosan or PSP-4-PVP polymer giving a 3D matrix containing the $IrCl_3$, compound linked to the polymeric chain. The following steps could involve the starting of the organic carbonization, producing holes where the nanoparticles begin to nucleate. As it was confirmed in earlier studies [12, 30], the IrO_2, grow over layered graphitic carbon host which is lost near to the final annealing temperature ie. 800 °C.

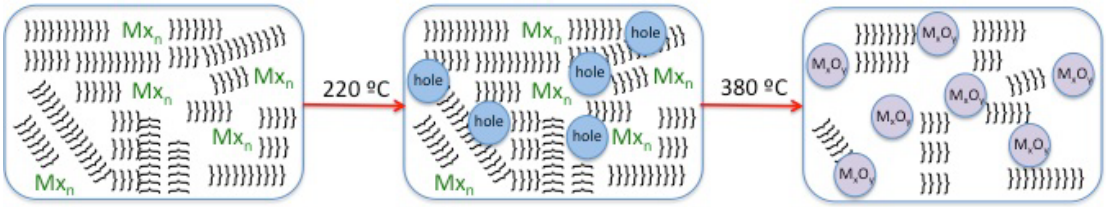

Fig. 10 Schematic representation of the proposed mechanism of formation of the metal oxide nanoparticles. MX_n represent the general formula of the metallic salt coordinated to the Chitosan polymer and }}}}}}} represent the polymeric Chitosan. The temperature are referential general values.

As for the incorporation of IrO_2 into SiO_2 matrices, no studies have been previously performed. We believe that SiO_2 is formed during the step of the formation of the Chitosan●$(IrCl_3)_X$ and PSP-4-PVP●$(IrCl_3)_X$ precursors, right after the incorporation of the TEOS($Si(OC_2H_5)_4$) in solution under hydrolysis conditions (see experimental section). Possibly, hydrolyzed rests such as $Si\text{-}OC_2H_5$ are forming solid precursors with a formula similar to Chitosan●$(IrCl_3)_X(SiO_2)y(Si\text{-}OC_2H_5)y\text{-}z$ and PSP-4-PVP●$(IrCl_3)_X$, were $(SiO_2)y(Si\text{-}OC_2H_5)y\text{-}z$ presents z anhydrous groups. These precursors form IrO_2 remaining inside the SiO_2 matrices, after their subsequent pyrolysis, as previously described.

4. Conclusions

A general solventless method using the easily synthetized precursors Chitosan●$(IrCl_3)_X$ and PSP-4-PVP●$(IrCl_3)_X$ affords the nucleation of IrO_2 nanoparticles. Incorporation of these metal oxide into SiO_2 matrix was achieved using a thermal treatment of the chitosan and PVP precursors, in order to give the $IrO_2//SiO_2$, composites. This composite was prepared for the first time. For all the composites, a regular distribution of the respective IrO_2 nanoparticles inside SiO_2 was observed. Photocatalytic degradation of MB using IrO_2 was measured for the first time, founding a moderate activity, observing no significant effect from both precursor studied polymers. Similar moderate photocatalytic activity was found for the $IrO_2//SiO_2$ composites. A possible future direction of the work involves the inclusion

of nanostructured IrO2 inside other matrices such as TiO2 and Al2O3, with the purpose to investigate the matrix effect on the optical and photodegradation properties. In addition, the idea is also to demonstrate the photodegradation properties of iridium oxide toward other dye contaminants as methyl orange.

ACKNOWLEDGMENTS

The authors acknowledge Fondecyt Project 1160241 for financial support. This research has also received funding from Consejo Superior de Investigaciones Científicas, Spain under grant I-COOP LIGHT 2015CD0013. The microscopy works have been conducted in the "Laboratorio de Microscopias Avanzadas" at "Instituto de Nanociencia de Aragon - Universidad de Zaragoza" . Authors acknowledge the LMA-INA for offering access to their instruments and expertise. The use of Servicio General de Apoyo a las Investigación (SAI, University of Zaragoza) and is finally acknowledged.

REFERENCES

[1] F. A. Cotton and G. Wilkinson, Advanced Inorganic Chemistry, Chapter 22 and 30; John Wiley and Sons: New York, 1980.

[2] R. Jin, The impacts of nanotechnology on catalysis by precious metal nanoparticles. Nanotechnology Rev. (2012) 31-56.

[3] M. Fernandez-Garcia, A. Martinez-Arias, J. Hanson, C. Rodriguez, Nanostructured Oxides in Chemistry: Characterization and Properties. J. A. Chem. Rev. 104 (2004) 4063-4104.

[4] R.S. Chen, A.Korotcov, Y.Sh. Huiang, D. Tsai, One-dimensional conductive IrO_2 nanocrystals Nanotechnology 17 (2006) 67-87.

[5] H. Woo, H.Sh. Shim, J.H. Myung, Ch. Lee, Annealing effect on the structural properties of IrO_2. Vacuum 82 (2008) 1400-1403.

[6] E. Ortel, T. Reier, P. Strasser, R. Kraehnert, Mesoporous film template by PEO-PB-PEO block-copolymers: Self-Assembly, Cristalization behaviour and electrocatalytic performance. Chem Mater. 23 (2011) 3201-3209.

[7] Y. Zhao, E.A. Hernandez, N.M. Vargas-Barbosa, J.L. Dysart, T.E. Mallouk, A high yield Synthesis of ligand-free iridium oxide nanoparticles with high electrocatalytic activity J. Phys.Chem.Lett. 2 (2011) 402-406.

[8] A. Brewer, D. Wicajksana, J. Maria, A. Kingon, S. Franzen, Investigation of the electrical and optical properties of iridium oxide by reflectance FTIR spectroscopy and density functional theory calculations. Chem.Phys. 313 (2005) 25-31.

[9] D. Xu, P. Diao, T. Jin, Q. Wu, X. Liu, X. Guo, H. Gong, F. Li, M. Xiang, Y. Ronghai, Iridium oxide nanoparticles and Iridium/Iridium Oxide Nanocompósites: Photochemical Fabrication and Application in Catalytic Rediction of Notrophenol. ACS Appl.Interfaces 7 (2015) 16738-16749.

[10] K. Biswas, C.N. Rao, Synthesis and characterization of Nano crystals of oxide metals RuO_2, IrO_2, and ReO_3. J. Nanosci. Nanotechniol. 7 (2007) 1969-1974.

[11] Y.M. Lee, J. Suntivich, K.J. May, E.E. Perry, H. Shao, Synthesis and activities of Rutile IrO_2 and RuO_2 nanoparticles for oxygen evolution in acid alkaline solutions. J. Phys.Chem.Lett. 2 (2011) 402-406.

[12] C. Díaz, M.L. Valenzuela, M.A. Laguna-Bercero, A. Orera, D. Bobadilla, S. Abarca, O. Peña, Synthesis and magnetic properties of nanostructured metallic Co, Mn and Ni

oxide materials obtained from solid-state metal-macromolecular complex precursors. RSC Advances 7 (2017) 27729-27736.

[13] C. Díaz, M.L. Valenzuela, K. Mendoza, O. Peña, C. O´Dwyer, Nanostructured copper oxides and phosphates from a new solid-state route. Inorg. Chimica Acta 377 (2011) 5-13.

[14] C. Díaz, O. Crespo, C. O´Dwyer, C. Gimeno, A. Laguna, I. Ospino, M.L. Valenzuela, Luminescent Gold and Silver Complexes with the Monophosphane 1-(PPh_2)-2-Me-$C_2B_{10}H_{10}$ and Their Conversion to Gold Micro-and Superstructured Materials. Inorganic Chemistry 54 (2014) 7260-7269.

[15] B. Teo, X. Sun, Silicon-based low-dimensional nanomaterial and nanodevices. Chem. Rev. 107 (2007) 1454-1532.

[16] G.B. Khomutov, V.V. Kislov, M.N. Antipirina, R.V. Gainutdinov, S.P. Gubin, A.Y. Obydenov, S.A. Pavlov, A.A. Rakhnyanskaya, A.N. Sergeev-Cherenkov, E.S. Soldatov, D.B. Suyatin, A.L. Toltikhina, A. S. Trifonov, T.V. Yurova, Interfacial nanofabrication strategies in development of new functional nanomaterials and planar supramolecular nanostructures for nanoelectronics and nanotechnology. Microelectronic Engineering 69 (2003) 373-383.

[17] M.P. Pileni, Self-Assembly of Inorganic Nanocrystals: Fabrication and Collective Intrinsic Properties. Accounts Chem. Res. 40 (2007) 685-693.

[18] M.P. Pileni, 2D superlattices and 3D supracrystals of metal nanocrystals: a new scientific adventure. J. Mat. Chem. 21 (2001) 16748-16758.

[19] Y. F. Wan, N. Goubet, P.A. Albouy, M.P. Pileni, Hierarchy in Au nanocrystal ordering in supracrystals: A potential approach to detect new physical properties. Langmuir 29 (2013) 7456-7463.

[20] C. Díaz, M.L. Valenzuela, Metallic Nanostructures Using Oligo and Polyphosphazenes as Template or Stabilizer in Solid State" in Encyclopedia of Nanoscience and Nanotechnology, Edited H.S.Nalwa. 16 (2010) 239-256.

[21] K. R. Reddy, CH. V. Reddy, M. N. Nadagouda, N. P. Shetti, S. Jaesool, T. M. Aminabhavi, Polymeric graphitic carbon nitride (g-C3N4)-based semiconducting nanostructured materials: Synthesis methods, properties and photocatalytic applications, J. Environ. Manag. 238 (2019) 25-40.

[22] V. N. Rao, N. L. Reddy, M. M. Kumari, P. Ravi, M. Sathish, K.M. Kuruvilla, V. Preethi, K. R. Reddy, N. P. Shetti, T. M. Aminabhavi, M.V. Shankara, Photocatalytic recovery of H2 from H2S containing wastewater: Surface and interface control of photo-

excitons in Cu2S@TiO2 core-shell nanostructures, Appl. Catal. B: Environ. 254 (2019) 174–185.

[23] Ch V. Reddy, I. N. Reddy, K. R. Reddy, S. Jaesool, K. Yoo, Template-free synthesis of tetragonal Co-doped ZrO2 nanoparticles for applications in electrochemical energy storage and water treatment. Electrochim. Acta 317 (2019) 416-426.

[24] G. Guidetti, E. A. A. Pogna, L. Lombardi, F. Tomarchio, I. Polishchuk, R. R. M. Joosten, A. Ianiro, G. Soavi, N. A. J. M. Sommerdijk, H. Friedrich, B. Pokroy, A. K. Ott, M. Goisis, F. Zerbetto, G. Falini, M. Calvaresi, A. C. Ferrari, G. Cerullo and M. Montalti, Photocatalytic activity of exfoliated graphite–TiO2 nanoparticle composites. Nanoscale 11 (2019) 19301–19314.

[25] W.Z. Li, D. Mei, M.H. Engelhard, F. Gao, J. Liu, Y. Wang, H.F. Peden, A General Mechanism for Stabilizing the Small Sizes of Precious Metal Nanoparticles on Oxide Support. Chem Mater. 26 (2014) 5475-5481.

[26] W.Z. Li, L Kovarich, D. Mei, Y. Wang, H.F. Peden, Stable Platinum nanoparticles on Specific $MgAl_2O_4$ spinel facets at high temperatures in oxidizing atmosphere Nature Commun. 4 (2013) 2481-2488.

[27] Sh. Liu, M. Han, C.Yang, Silica-Coated Metal Nanoparticles. Asian J. 5 (2010) 36-45.

[28] M. Momeni, H. Saghafian, F. Golestani-Fard, N. Barati, A. Khanahmadi, Effect of SiO2 addition on photocatalytic activity, water contact angle and mechanical stability of visible light activated TiO2 thin films applied on stainless steel by a sol gel method. Appl. Surf. Sci. 392 (2017) 80-87.

[29] P. Zhang, J. Tian, R. Xu, G. Ma, Hydrophilicity, photocatalytic activity and stability of tetraethyl orthosilicate modified TiO_2 film on glazed ceramic surface. Appl. Surf. Sci. 266 (2013) 141-147

[30] J. Yu, J. Yu, X. Zhao, The effect of SiO2 addition on the grain size and photocatalytic activity of TiO2 thin films. J. Sol-Gel Sci. Technol., 24 (2002) 95-103

[31] C. Díaz, M.L. Valenzuela, Small Molecule and High Polymeric Phosphazenes Containing Oxypyridine Side Groups and Their Organometallic Derivatives: Useful Precursors for Metal Nanostructured Materials. Macromolecules 39 (2006) 103-111.

[32] Y. Li, Y. Hu, H. Jiang, Ch. Li, Double-faced γ-Fe_2O_3//SiO_2 nanohybrid: flame synthesis , in situ selective modificacion and highly interfacial activity. Nanoscale 5 (2013) 5360-5367.

[33] Y. Kuwahara, N. Furuichi, H. Seki, H. Yamashita, One-pot synthesis of molybdenum oxide nanoparticles encapsulated in hollow silica sphreres: an efficient and reusable catalyst for epoxication of olefins. J. Mater. Chem. A 5 (2017) 18518-18526.

[34] M. Tamura, K. Tokonami, Y. Nakagawa, K. Tomishige, Effective NbO_X-Modified Ir/SiO_2 catalyst for selective gas-phase hydrgenattion of crotonaldehyde to crotykl alcohol. ACS Sustainable Chem. Eng. 5 (2017) 3685-3697.

[35] C. Wang, J. Li, X. Liang, Y. Zhang and G. Guo, Energy Environ. Sci. 7 (2014) 2831–2867.

[36] S. P. Dharupaneedi, S. K. Nataraj, M. Nadagouda, K. R. Reddy, S. S. Shukla, T. M. Aminabhavi, Membrane-based separation of potential emerging pollutants. Separation and Purification Technology 210 (2019) 850–866.

[37] K. R. Reddy, V. G. Gomes and M. Hassan, Carbon functionalized TiO2 nanofibers for high efficiency photocatalysis. *Mater. Res. Express* **1 (**2014) 015012.

[38] L. Barrientos, P. Allende, M. Á. Laguna-Bercero, J. Pastrián, J. Rodriguez-Becerra, L. Cáceres-Jensen, Controlled Ag-TiO2 heterojunction obtained by combining physical vapor deposition and bifunctional surface modifiers, J. Phys. Chem. Solids 119 (2018) 147-156.

[39] C. Díaz, M.L. Valenzuela, V. Lavayen, C. O'Dwyer, Layered Graphitic Carbon Host Formation during Liquid-free Solid State Growth of Metal Pyrophosphates. Inorg. Chem. 51 (2012) 6228-6236.